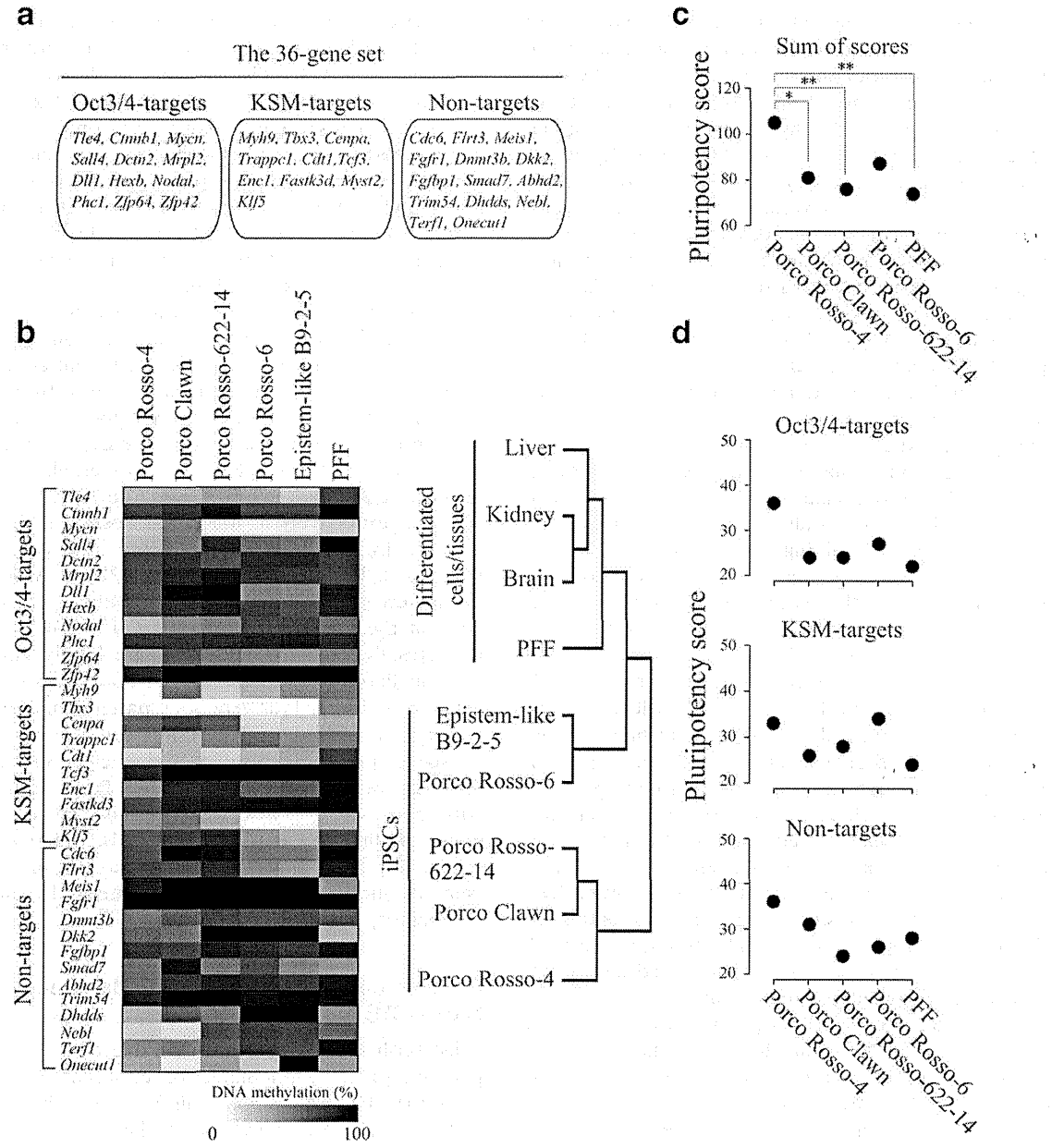

FIG. 1. DNA methylation profiles of porcine iPSCs. (**a**) The 36-gene set analyzed for DNA methylation profiling of porcine iPSCs. The genes were retrieved from EShypo-T-DMRs previously determined in mouse ESCs, and were categorized into three groups: Oct3/4-targets, KSM-targets, and non-targets. (**b**) DNA methylation status of the 36-gene set in five iPSC lines (Porco Rosso-4, Epistem-like B9-2-5, Porco Rosso-6, Porco Rosso-622-14, and Porco Clawn) and porcine fetal fibroblast (PFF) by COBRA assay. The methylation level is represented as a heatmap (left panel). Based on the methylation level determined by COBRA assay, differentiated cell or tissues (brain, liver, kidney, and PFF) and five porcine iPSC lines were clustered according to the similarity of their DNA methylation profiles at the 36 selected genes using the Euclidean distance (right panel). (**c**) Sum of pluripotency scores of the 36 genes for porcine naïve-like iPSCs and PFF. Depending on percentage difference in methylation levels between blastocysts and iPSCs, pluripotency scores for each gene were classified into five categories: $<20\%$, 20–40%, 40–60%, 60–80%, or $>80\%$, with pluripotency scores of 5, 4, 3, 2, or 1, respectively. Total scores of the 36-gene set are plotted. Statistical comparison was performed by Wilcoxon test. $^{*}P<0.05$; $^{**}P<0.01$. (**d**) Pluripotency scores of porcine iPSCs and PFF for each of the three gene-groups. Total scores of the genes belonging to each group (Oct3/4-targets, KSM-targets, and non-targets) are plotted.

porcine genes orthologous to mouse genes with EShypo-T-DMRs, whose DNA methylation levels were low in mouse ESCs but 30% or more higher in differentiated tissues/cells (Sato *et al.*, 2010). However, 16 of these were found to be hypomethylated in porcine somatic tissues, and further, four genes were hypermethylated in porcine blastocysts, consisting of pluripotent cells (Supporting Information Fig. 1). Therefore, these 20 genes were excluded, and the remaining 36 were used for DNA methylation analyses. Among these 36 genes, several are known to be hypomethylated in mouse ESCs, but to be in a poised state of transcriptional activation, rather than actively expressed. This type of epigenetic regulation has been reported in H3K4me3/H3K27me3-enriched bivalent regions (Meissner *et al.*, 2008; Xu *et al.*, 2007).

We performed DNA methylation analyses of the 36 selected genes in five porcine iPSC lines; Porco Rosso-4, −6, −622-14, Epistem-like B9-2-5, and Porco Clawn. Epistem-like B9-2-5 was cultured in typical non-mouse ESC/iPSC media containing bFGF (Fujishiro *et al.*, 2013), and its colony shape and gene expression patterns were similar to those of mouse epiblast stem cells (EpiSCs; Brons *et al.*, 2007; Tesar *et al.*, 2007). The other four cell lines were cultured with porcine LIF, and their colony shape was similar to that of mouse ESCs (Fujishiro *et al.*, 2013). DNA methylation levels of the 36 genes were examined by combined bisulfite restriction analysis (COBRA) assay (Xiong and Laird, 1997) in iPSCs and porcine fetal fibroblast (PFF) used to produce the iPSC lines (Fig. 1b, left panel). Hierarchical clustering of DNA methylation status was performed on the basis of the 36-gene set for somatic cells/tissues and iPSC lines (Fig. 1b, right panel). Somatic tissues (brain, liver, and kidney) and PFF clustered together, whereas the five iPSC lines clustered separately, indicating that the DNA methylation profile of the 36-gene set could distinguish between differentiated cells/tissues and iPSCs.

Next, we determined a "Pluripotency score" based on comparison of methylation levels of the 36 genes between blastocysts consisting of pluripotent cells and the four naïve-like iPSC lines. Since Epistem-like B9-2-5 is distinguishable from naïve-like iPSC lines based on the mouse EpiSC-like colony shape and bFGF-dependent proliferation (Fujishiro *et al.*, 2013), Epistem-like B9-2-5 was excluded in the following experiments. Scoring was performed for each gene, and the sum of the scores of the 36 genes was plotted (Fig. 1c). In this way, high pluripotency scores are awarded to iPSC lines with DNA methylation profiles close to those of pluripotent cells. Among the four iPSC lines examined, Porco Rosso-4 showed the highest pluripotency score, which was statistically significant when compared with PFF, Porco Rosso-622-14, and Porco Clawn. We further examined the pluripotency score depending on the gene groups (Oct3/4-targets, KSM-targets, or non-targets; Fig. 1d). The Oct3/4-target genes had higher pluripotency scores in the Porco Rosso-4 cell line (36) than the other three cell lines and PFF (22–27). This tendency was also observed for non-target genes. By contrast, the score of KSM-target genes in Porco Rosso-4 was similar to that of Porco Rosso-6. Thus, among the four iPSC lines examined, the DNA methylation profile of Porco Rosso-4 is most similar to that of pluripotent cells. This was consistent with the results of the hierarchical clustering analysis, where the Porco Rosso-4 line was separate from the Epistem-like B9-2-5 line.

We confirmed the DNA methylation status of six gene loci (*Ctnnb1*, *Sall4*, *Tle4*, *Dll1*, *Enc1*, and *Nebl*), whose DNA methylation level was clearly different among the examined iPSC lines (Fig. 1b, left panel), by bisulfite sequencing. All 6 gene loci were hypermethylated in PFF and liver, whereas hypomethylated status was observed in blastocysts (Fig. 2). DNA methylation levels of the Oct3/4-target genes, *Ctnnb1* and *Sall4*, were 24 and 2%, respectively in the Porco Rosso-4 line, which had the highest pluripotency score among the four iPSC lines. However, Porco Rosso-622-14, which had the lowest pluripotency score, exhibited hypermethylation at the *Ctnnb1* (65%) and *Sall4* (61%) loci. This indicates that *Ctnnb1* and *Sall4* are highly demethylated in Porco Rosso-4 but not in Porco Rosso-622-14 cells. At the other four gene loci, partial demethylation was also observed in Porco Rosso-4 but not Porco Rosso-622-14. These bisulfite sequencing results confirm that, in Porco Rosso-4 iPSC line, DNA methylation patterns of the 6 genes, we analyzed changed to the expected direction as pluripotent cells, and Oct3/4-target genes, *Sall4* and *Ctnnb1*, especially underwent demethylation within the entire sequenced regions in the majority of the cell population.

Contribution of Porcine iPSCs to the Inner Cell Mass (ICM) of Blastocysts

Established iPSC lines are intended for use in transplantation and complementation experiments. Considering that the naïve-like iPSC lines do not differ greatly in terms of morphology and marker gene expression (Fujishiro *et al.*, 2013), it is more appropriate to select candidate iPSC lines using different indices. We next investigated contribution of the iPSC lines to the ICM of blastocysts using the aggregation method (Fig. 3a). We performed two independent experiments (Exps. 1 and 2), and found that Porco Rosso-4 cells contributed better to the ICM compared with Porco Rosso-622-14 in both experiments (Fig. 3b). In Exps. 1 and 2, the number of embryos that exhibited ICM contribution of iPSCs statistically differed between Porco Rosso-4 (14/57, 24.6%) and Porco Rosso-622-14 (2/51, 3.9%; Fig. 3c). The sum of pluripotency scores (105) for the three gene groups (Oct3/4-targets, KSM-targets, and non-targets) for Porco

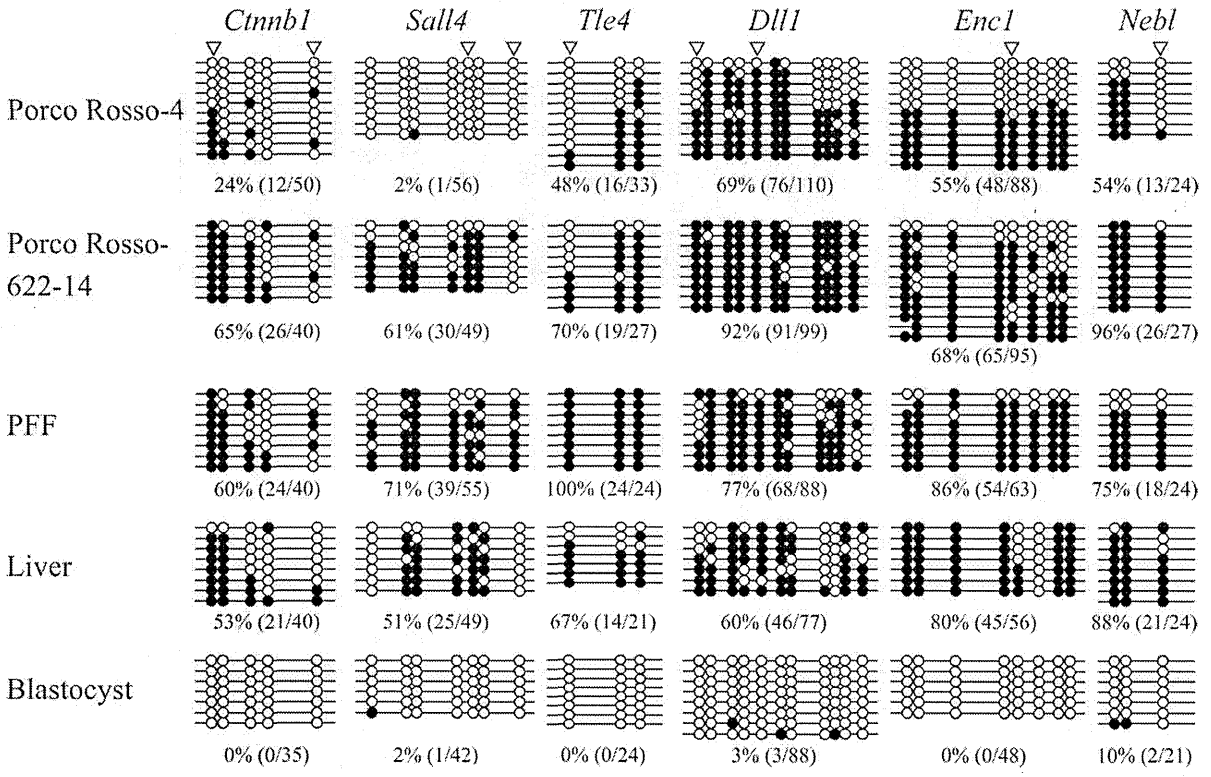

FIG. 2. DNA methylation status of EShypo-T-DMRs in iPSCs (Porco Rosso-4 and Porco Rosso-622-14) analyzed by sodium bisulfite sequencing. Open and closed circles indicate unmethylated and methylated CpG dinucleotides, respectively. Arrowheads indicate CpG sites analyzed by COBRA assay. The methylation level (%) was based on the methylated CpGs/all examined CpGs.

Rosso-4 was higher than that of Porco Rosso-622-14 (76), indicating that a higher pluripotency score coincides with higher efficiency of incorporation of iPSCs into the ICM. Thus, the pluripotency score based on the DNA methylation status of the 36 genes provides a feasible index for evaluating porcine iPSCs.

DNA Methylation Analysis in huKO-Negative Cells

We previously reported that approximately 5% of the cell population in Porco Rosso-4 became negative for humanized Kusabira-Orange (huKO) fluorescence (huKO-negative cells), and their characteristics were closer to those of the expected pluripotent cells (Fujishiro *et al.*, 2013). This implies that high-quality porcine iPSCs were enriched in huKO-negative fraction. To confirm whether the DNA methylation profile of EShypo-T-DMRs is a useful index for screening porcine iPSCs, we analyzed the DNA methylation status of huKO-negative cells. The huKO-negative cells in Porco Rosso-4 were collected by cell sorting, together with cells with high expression of huKO (huKO positive; Fig. 4a). EShypo-T-DMRs (*Dll1* and *Enc1*) were analyzed by bisulfite sequencing, because approximately half of the sequenced clones exhibited obvious hypomethylation in Porco Rosso-4 (Figs. 2 and 4), suggesting that Porco Rosso-4 contains a certain proportion of the cells properly demethylated at these two loci. Based on the bisulfite sequence data (Fig. 4b), the percentage of the cells hypomethylated at these two loci in Porco Rosso-4 was calculated on the basis of the number of unmethylated CpGs in the sequenced clones before and after sorting (Fig. 4c). Before sorting, the percentages of hypomethylated cells at the *Dll1* and *Enc1* loci were estimated as 36% and 50%, respectively. In huKO-negative fraction, 67–80% of the cells were considered as hypomethylated, whereas the proportion of hypomethylated cells in the huKO-positive fraction were lower than that of the cells before sorting, indicating that huKO-negative cells were hypomethylated at these EShypo-T-DMRs as expected from the DNA methylation patterns in mouse ESCs. Thus, the DNA methylation profile based on the EShypo-T-DMRs reflects the characteristics of the expected cells.

Improvement of Pluripotency Scores of Porcine iPSCs by SF + 2i Treatment

It is known that treatment with two signal-transduction inhibitors (2i) of PD0325901, an inhibitor of mitogen-activated protein kinase/extracellular signal-

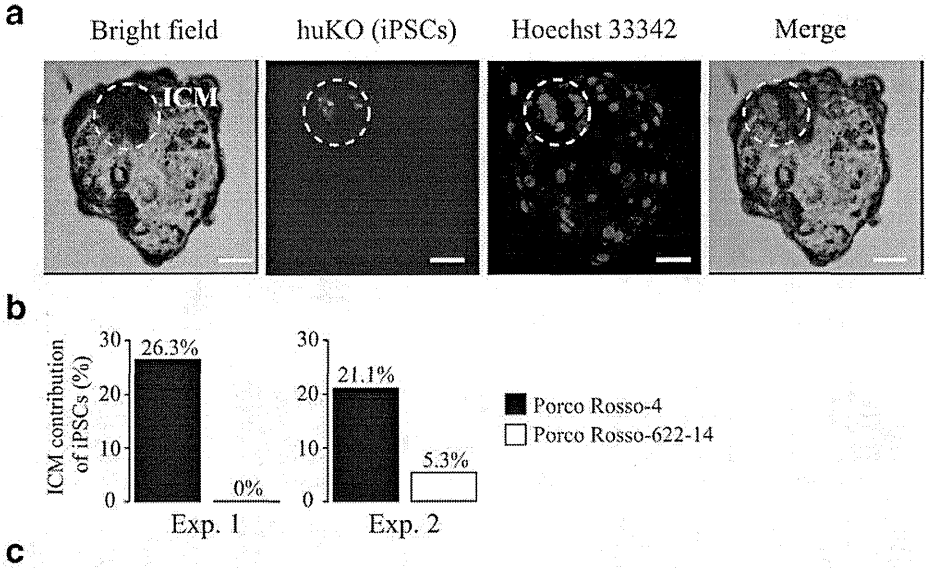

c

Donor cell	n	Developed to blastocyst	Number of * blastocysts analyzed	Contribution to ** ICM	Sum of *** pluripotency score (/180)
Porco Rosso-4	345	280/345 (81.2%)	57	14/57[a] (24.6%)	105
Porco Rosso-622-14	146	123/146 (84.2%)	51	2/51[b] (3.9%)	76
ICM	50	46/50 (92.0%)	46	37/46 (80.4%)	–

ab, $p<0.01$ (chi-square test)
*, The other blastocysts were used for different experiments.
**, Porco Rosso-4, n=38 (Exp. 1) and n=19 (Exp. 2). Porco Rosso-622-14, n=13 (Exp. 1) and n=38 (Exp. 2).
***, Pluripotency score was calculated only for iPSCs.

FIG. 3. Contribution of iPSCs to the ICM of blastocysts. (**a**) Porcine iPSCs (Porco Rosso-4 and Porco Rosso-622-14) were aggregated with porcine parthenogenetic 4- to 8-cell-, or morula-stage embryos. After in vitro culture, contribution of iPSCs to blastocysts was analyzed by fluorescence of the transgene, humanized Kusabira-Orange (huKO). Scale bar = 50 μm. (**b**) The percentage of ICM contribution of Porco Rosso-4 and Porco Rosso-622-14. Aggregation experiments using porcine iPSCs (Porco Rosso-4 and Porco Rosso-622-14) were performed twice independently (Exps. 1 and 2). (**c**) Summary of the contribution of iPSCs to the ICM of blastocysts. Using the ICM cells dissociated from blastocysts as donor cells, most aggregated embryos developed into blastocysts, and donor ICM cells could contribute efficiently to the ICM of the host blastocyst, confirming the contribution of pluripotent cells to the ICM. Statistical comparison was performed by chi-square test.

regulated kinase (ERK) kinase (MEK), and CHIR99021, an inhibitor of GSK3β, is effective for establishment of a naïve state in iPSCs from rodent and human (Buehr *et al.*, 2008; Hanna *et al.*, 2009; Li *et al.*, 2008). Additionally, 2i treatment has been shown to improve the characteristics of porcine iPSCs (Rodríguez *et al.*, 2012). We examined whether the DNA methylation profile of the 36 selected genes is a useful index for evaluation of the changes in characteristics of porcine iPSCs after 2i treatment. We analyzed the DNA methylation status of Porco Clawn cultured in medium with FBS, or in serum-free (SF) or in SF+2i medium, by COBRA assay (Fig. 5a, left panel). Cells treated with 5-aza-2′-deoxycytidine (5-aza-dC), an inhibitor of DNA methyltransferase 1, were also analyzed for DNA methylation status.

In the course of mouse iPSC establishment, promoter regions of pluripotency-related genes, including EShypo-T-DMRs become demethylated (Okita *et al.*, 2007; Sato *et al.*, 2010; Takahashi and Yamanaka, 2006). In this study, we observed that porcine iPSCs cultured under SF conditions exhibited effective demethylation of the Oct3/4-target genes compared with FBS-cultured cells (Fig. 5a, right panel). In addition, the number of demethylated and reprogrammed genes was greatly increased under the SF+2i condition. These tendencies were also observed in the KSM-target and non-target gene groups, suggesting that SF+2i condition induced demethylation of the 36 selected genes. However, 5-aza-dC treatment was not effective, and the number of hypomethylated Oct3/4-target genes

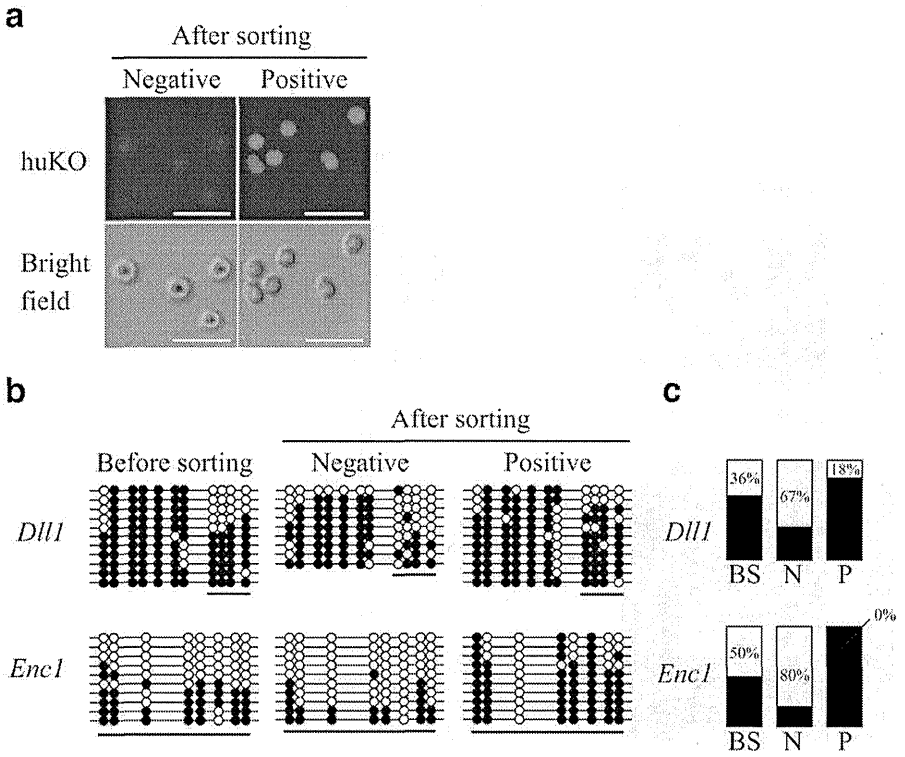

FIG. 4. DNA methylation status of huKO-negative cells after sorting of Porco Rosso-4. (**a**) The huKO-negative and huKO-positive cells of Porco Rosso-4 iPSC line after sorting. Scale bar = 50 μm. (**b**) DNA methylation status of *Dll1* and *Enc1* before and after sorting (huKO-negative and huKO-positive). Open and closed circles indicate unmethylated and methylated CpG dinucleotides, respectively. (**c**) The percentage of (hypomethylated clones)/(all sequenced clones) in the underlined regions of Figure 4b. Hypomethylated clones were defined on the basis of the number of unmethylated CpGs underlined below the circles in each sequenced clone. At the *Dll1* locus, the DNA methylation statuses of four CpGs were clearly different between the bulk Porco Rosso-4 line and PFF in Figure 2, whereas the other CpGs were almost fully methylated in all of the sequenced clones, indicating that the methylation statuses of the four selected CpGs in the underlined region were informative enough for evaluating the ratio of properly reprogrammed cells in huKO-negative and huKO-positive fractions. Thus, sequenced clones with three or more unmethylated CpGs in the four CpGs were designated as hypomethylated at the *Dll1* locus. At the *Enc1* locus, about half of the sequenced clones exhibited six or more unmethylated CpGs within the eight CpGs examined in the bulk Porco Rosso-4 line (Fig. 2). However, the other sequenced clones were almost fully methylated at the eight CpGs. Thus, sequenced clones exhibiting six or more unmethylated CpGs were designated as hypomethylated to strictly evaluate properly reprogrammed cells at the *Enc1* locus. With respect to the other four EShypo-T-DMRs (*Ctnnb1*, *Sall4*, *Tle4*, and *Nebl*) analyzed in Figure 2, the DNA methylation statuses of hypomethylated CpGs in bulk Porco Rosso-4 cells did not differ between huKO-negative and huKO-positive cells (Supporting Information Fig. 2). Black and white bars indicate the ratio of hypermethylated and hypomethylated clones, respectively. BS, before sorting; N, huKO-negative cells; P, huKO-positive cells.

remained unchanged compared with FBS-cultured controls.

Improvement of the DNA methylation status of Porco Clawn cells by culture under SF+2i conditions was confirmed by sodium bisulfite sequencing (Fig. 5b). *Sall4*, *Hexb*, and *Zfp64*, all of which are Oct3/4-targets, were hypermethylated in the presence of FBS, whereas demethylation occurred under the SF+2i conditions. By contrast, demethylation at *Hexb* and *Zfp64* was much less pronounced in the 5-aza-dC-treated cells (Fig. 5b). These results suggest that the SF+2i condition was the most effective of those tested for reprogramming of the 36-gene set. Demethylation also occurred in the SF+2i-treated cells at the *Dll1* and *Enc1* loci (Supporting Information Fig. 3a), whereas a portion of cells remained hypermethylated at the *Dll1* locus (Supporting Information Fig. 3b). In addition, DNA methylation analysis revealed that a proportion of cells still needed to be reprogrammed at the *Enc1* locus even after SF+2i treatment.

To examine whether SF+2i culture conditions are effective in improving pluripotency scores, we cultured Porco Clawn, in addition to several other iPSC lines, under the same conditions (FBS, SF, and SF+2i), and DNA methylation status was analyzed by COBRA assay (Fig. 5c). Of note, the pluripotency scores of all the three gene groups (Oct3/4-targets, KSM-targets, and non-targets) were increased in Porco Rosso-4 cells under SF+2i condition compared with FBS, or SF

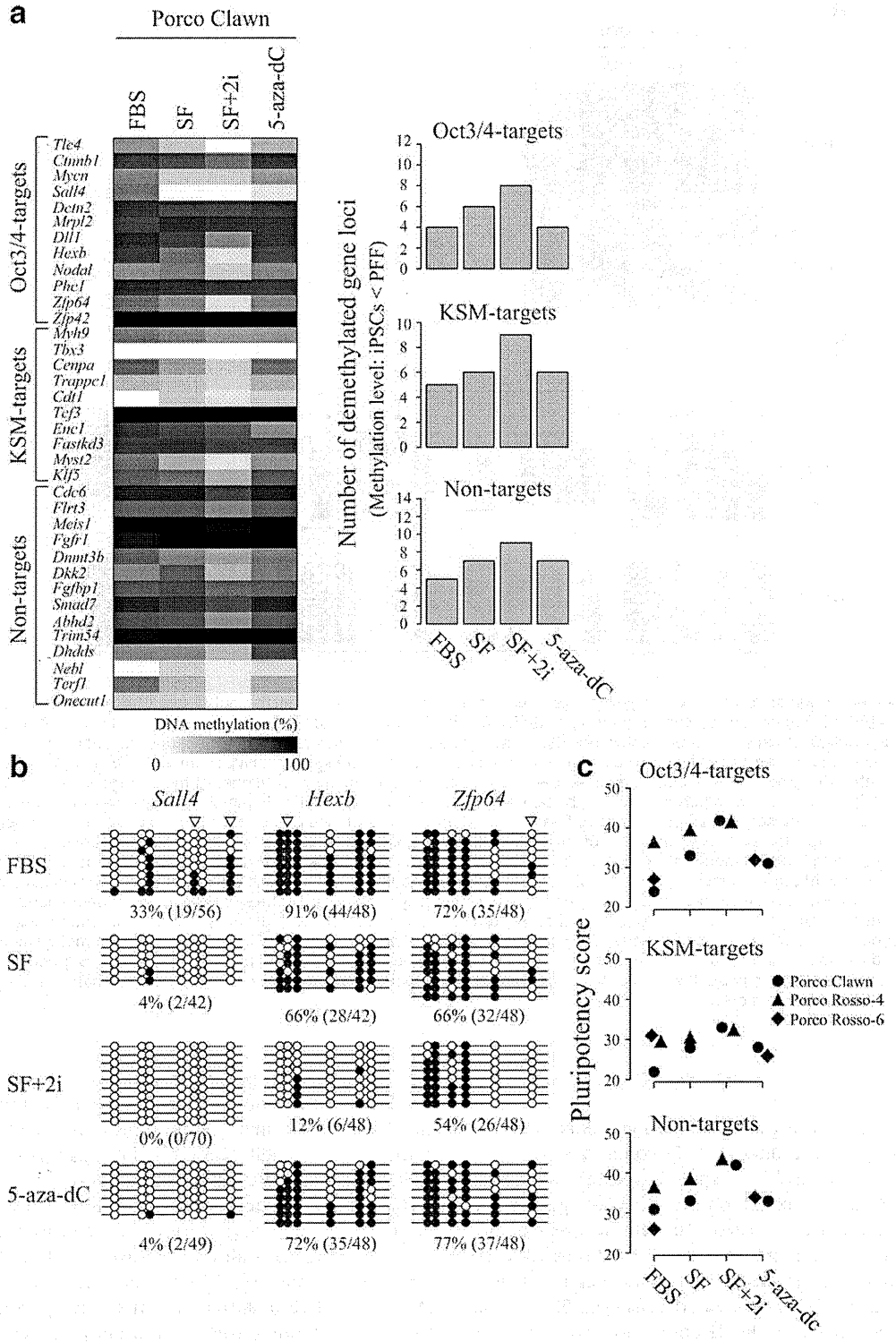

FIG. 5. Continued

conditions. Thus, SF+2i treatment is effective for multiple porcine iPSC lines.

DISCUSSION

The porcine iPSCs analyzed in this study exhibited LIF-dependent self-renewal and a round morphology, similar to mouse ESCs (Fujishiro *et al.*, 2013). The expression patterns of several pluripotency-related marker genes, including *Oct3/4*, were also similar among the iPSC lines. As it is intended that these iPSC lines will be used for applications such as chimera formation (Okita *et al.*, 2007) and transplantation experiments (Kobayashi *et al.*, 2010; Usui *et al.*, 2012), it is important that they are able to contribute to the ICM of the blastocyst embryos. In this context, a simple index, other than morphology and marker gene expression, correlating with ICM contribution efficiency is required to allow pre-screening to determine which iPSC lines are appropriate for use in labor- and cost-intensive transplantation experiments. We previously reported that mouse iPSC lines with high chimera-forming ability (Aoi *et al.*, 2008) have DNA methylation profiles close to those of ESCs (Sato *et al.*, 2010). In this study, we focused on the DNA methylation profile of mouse EShypo-T-DMRs and determined a 36-gene set applicable to porcine iPSC lines. The pluripotency scores, based on the DNA methylation profile of the 36-gene set, were revealed to differ among iPSC lines that were indistinguishable by morphology or marker gene expression. Moreover, the iPSC line with the highest pluripotency score contributed to the ICM as assessed by a chimera formation experiment, whereas the iPSC line with the lowest score contributed much less efficiently to the ICM. Collectively, the DNA methylation profile of the 36-gene set derived from mouse EShypo-T-DMRs correlated with the ability to contribute to the ICM of blastocyst embryos.

In the course of mouse iPSC establishment, reprogramming for activation is important for genes such as endogenous *Oct3/4* and target genes of Yamanaka factors (Oct3/4, Sox2, Klf4, and c-Myc) (Okita *et al.*, 2007; Takahashi and Yamanaka, 2006). In this study, we categorized the 36-gene set into three groups (Oct3/4-targets, KSM-targets, and non-targets), and analyzed DNA methylation status in porcine iPSCs. Among the three groups, differences in pluripotency score were most apparent in the Oct3/4-target genes. The Oct3/4-target group contains genes that are important for the maintenance of pluripotency in stem cells. For example, *Sall4* is an Oct3/4-target gene (Chen *et al.*, 2008; Sakaki-Yumoto *et al.*, 2006; Tsubooka *et al.*, 2009) and was hypomethylated in the porcine iPSC line exhibiting both a high pluripotency score and efficient contribution to ICM. Differences in pluripotency scores among the examined iPSC lines were less significant in the KSM-target group than the Oct3/4-target group. Non-target genes can be thought of as downstream targets of the four Yamanaka factors, thereby non-target genes should be secondarily reprogrammed after activation of the primary targets of the Yamanaka factors. Thus, the pluripotency score of non-target genes was relatively high in iPSCs with high Oct3/4- and KSM-target scores, most likely indicating the activation of the primary target genes. Therefore, although pluripotency scores of Oct3/4-target genes can be considered as the most important index for evaluation of porcine iPSCs, the DNA methylation profiles of all three groups making up the 36 genes are required for evaluation with high accuracy.

For establishing mouse iPSCs, 2i treatment has been reported as effective for obtaining high-quality lines (Buehr *et al.*, 2008; Hanna *et al.*, 2009; Li *et al.*, 2008). The 2i consists of MEK- and GSK3b-inhibitors, both of which prevent differentiation of mouse ESCs. In the porcine iPSC lines we examined, 2i-treatment effectively induced demethylation of the 36-gene set, with a consequent increase in pluripotency scores. Since an increased pluripotency score indicates cells with closer characteristics to those of pluripotent stem cells, such as mouse ESCs, the DNA methylation profile of the 36-gene set is useful for detection of improvements of porcine iPSC lines. In contrast, treatment of 5-aza-dC was less effective for improvement of pluripotency scores, implying that simple DNA demethylation by such compounds is insufficient. Taken together, DNA methylation profiling is useful for evaluation of characteristic changes of porcine iPSCs.

Reprogramming of endogenous pluripotency-related genes such as *Oct3/4* is crucial for stably maintaining iPSCs. By contrast, the first report of mouse iPSCs (Fbx15 iPSCs) observed incomplete demethylation of the endogenous *Oct3/4* region and the cells were not transmitted through the germline (Takahashi and Yamanaka, 2006), whereas superior germline-transmittable iPSC lines (Nanog iPSCs) showed complete demethylation of

FIG. 5. Improvement of DNA methylation status under different culture conditions. (**a**) DNA methylation status of Porco Clawn cells cultured in the presence of FBS, or in serum-free (SF), SF + 2i, or 5-aza-dC conditions was analyzed by COBRA assay; the methylation level is represented as a heatmap (left panel). The number of demethylated genes in each culture condition is shown in the right panel. (**b**) DNA methylation status of three Oct3/4-target genes (*Sall4*, *Hexb*, and *Zfp64*) in Porco Clawn cells cultured under different conditions analyzed by sodium bisulfite sequencing. Open and closed circles indicate unmethylated and methylated CpG dinucleotides, respectively. Arrowheads indicate CpG sites analyzed by COBRA assay. The methylation level (%) was calculated as methylated CpGs/all examined CpGs. (**c**) DNA methylation status in Porco Rosso-4 cells cultured under SF or SF + 2i conditions and in Porco Rosso-6 cultured in the presence of 5-aza-dC was analyzed by COBRA assay. Pluripotency scores of the iPSC lines cultured under each condition were plotted for the three gene-groups (Oct3/4-targets, KSM-targets, and non-targets).

the endogenous pluripotency-related genes including *Oct3/4* (Okita *et al.*, 2007). We previously reported that the endogenous *Oct3/4* promoter region was relatively hypermethylated in the same porcine iPSC lines that were examined in this study (Fujishiro *et al.*, 2013). However, one iPSC line that we analyzed contained cells showing reprogrammed and hypomethylated status within the whole examined endogenous *Oct3/4* locus, suggesting that a small population of the cells were activated at the endogenous *Oct3/4* locus. In mouse ESCs, a 1.5-fold increase or two-fold decrease in endogenous *Oct3/4* expression led to cellular differentiation (Niwa *et al.*, 2000). Therefore, the appropriate expression level of endogenous *Oct3/4* is important for maintenance of pluripotency. In the pig, however, no *bona fide* pluripotent stem cells, such as mouse ESCs, have been described to date; thus, the appropriate expression level of endogenous *Oct3/4* remains to be determined. Based on the bisulfite sequencing data of endogenous *Oct3/4* in our previous study (Fujishiro *et al.*, 2013) and several Oct3/4-targets in this study, a proportion of the cells appear to be properly reprogrammed in the iPSC lines we examined. In addition, the finding that huKO-negative cells, which are likely closer to pluripotent cells (Fujishiro *et al.*, 2013), exhibited hypomethylation of EShypo-T-DMRs compared with the bulk iPSC line further support the usefulness of DNA methylation profile. Thus, DNA methylation analysis can evaluate the ratio of properly reprogrammed cells in each iPSC line without reference cells such as ESCs in the case of mouse iPSCs.

The porcine iPSC lines examined in this study were likely heterozygous and contained both properly and improperly reprogrammed cells, even after SF/2i-treatment, as shown by the measurement of the DNA methylation patterns of several EShypo-T-DMRs. For aggregation experiments, one iPSC colony large enough to be picked up was dissociated into single cells and aggregated with early embryonic cells. Under the present culture conditions, properly reprogrammed cells such as huKO-negative cells, which we proved to have better characteristics as stem cells (Fujishiro *et al.*, 2013), exhibited slower proliferation than improperly reprogrammed cells (data not shown). This implies that visible iPSC colonies, which can be used for aggregation experiments to analyze ICM contribution, contain substantial numbers of improperly reprogrammed cells due to higher proliferation potential than properly reprogrammed cells. Thus, the data demonstrating the ICM contribution of iPSCs in this study may have underestimated the ratio of properly reprogrammed cells that could be deduced from DNA methylation analysis. In this study, we identified several genes whose methylation profiles could be used to evaluate the ratio of properly reprogrammed cells. Thus, we will be able to identify appropriate culture conditions for the maintenance of properly reprogrammed cells by using the DNA methylation profiles of these genes.

In this study, we focused on the DNA methylation profile of the 36-gene set derived from EShypo-T-DMRs and established a new index for evaluation of porcine iPSCs correlating with their efficient contribution to the ICM of blastocysts. We provide proof-of-principle of the concept that mouse EShypo-T-DMR information is applicable to evaluate porcine iPSC lines. The gene set we used in this study is effective on validation of stemness under in vitro culture condition and in blastocyst stage embryos as one aspect of pluripotency. However, the other aspect of pluripotency to have broad lineage potential is also important but cannot be assessed by the gene set used in this study. We previously identified differentiated-tissue-specific hypomethylated loci (Tissuehypo-T-DMRs), which are related to certain specific somatic cell lineages and are hypermethylated in mouse ESCs (Sato *et al.*, 2010). By selecting another porcine gene set from Tissuehypo-T-DMRs in addition to the 36-gene set examined in this study, we will be able to perform more strict evaluation of porcine iPSCs in terms of pluripotency of both stemness and broad lineage potential. Since our previous findings indicated that hundreds of mouse EShypo- and Tissuehypo-T-DMRs could be used for evaluation of mouse iPSCs, we anticipate deriving further information about EShypo- and Tissuehypo-T-DMRs in multiple porcine iPSC lines with higher accuracy using next generation sequencer to perform ultra-deep bisulfite sequencing.

In conclusion, information regarding DNA methylation derived from mouse EShypo-T-DMRs is a feasible index for evaluation of porcine iPSCs as a pre-screening tool, distinct from morphology and marker gene expression analysis. Evaluation of porcine iPSC lines by DNA methylation analysis is simple and time/cost-saving. The concept of evaluation of iPSCs by DNA methylation profile is readily applicable to other mammalian cells, including human iPSCs/ESCs, which cannot be evaluated by chimera formation for ethical reasons.

METHODS

Animal Care

All of the animal experiments in this study were approved by the Institutional Animal Care and Use Committee of Meiji University (IACUC-11-1).

Chemicals

Chemicals were purchased from the Sigma Chemical Co. (St. Louis, MO), unless otherwise indicated.

Porcine iPSCs

Establishment of porcine iPSCs was described previously (Fujishiro *et al.*, 2013). Porcine iPSC lines, Porco

Rosso-4, −6, −622-14, and Epistem-like B9-2-5, expressing humanized Kusabira-Orange (huKO) were derived from PFF of huKO-transgenic pigs (Matsunari *et al.*, 2008). Porco Clawn iPSC line was derived from PFF of Clawn miniature pigs (Japan Farm, Kagoshima, Japan). All the iPSC lines were maintained in knockout DMEM medium (Invitrogen, Rockville, MD) containing 15% fetal bovine serum (FBS, Invitrogen) or knockout serum replacement (KSR, Invitrogen), 1% NEAA (Invitrogen), 1% glutamax-L (Invitrogen), 100 μM 2-mercaptoethanol (Invitrogen), 50 U/ml penicillin, 50 μg/ml streptomycin, 10 μM forskolin (Biomol, Farmingdale, NY), and 0.5% porcine LIF with or without 5 μM 5-aza-2′-deoxycytidine (5-aza-dC) for 10 days and two signal-transduction inhibitors (2i) of 0.5 μM PD0325901 and 3 μM CHIR99021 for three weeks on MMC-treated STO cells. huKO-negative and huKO-positive cells of Porco Rosso-4 were sorted by BD FACS Aria (Becton Dickinson, NJ).

COBRA Assay and Sodium Bisulfite Genomic Sequencing

DNA methylation analysis by COBRA assay was performed based on our previous results (Sato *et al.*, 2010) focusing on 58 genes that were hypomethylated in mouse ESCs. Genomic DNA was purified using the DNeasy Blood & Tissue Kit (Qiagen, Hilden, Germany), and digested with a restriction enzyme *Hind* III (Takara Bio, Shiga, Japan). Digested genomic DNA was purified with a QIAquick Gel Extraction Kit (Qiagen), and bisulfite reactions were performed using the EZ DNA Methylation-Direct Kit (Zymo Research, Irvine, CA). Bisulfite-treated DNA was amplified with BioTaq HS DNA polymerase (Bioline, London, UK) using specific gene primers (Supporting Information Table 1). Primer sequences are based on the porcine genome assembly, Sscrofa9.2 (November 2009 build) from the UCSC genome database. PCR was performed under the following conditions: 95°C, 10 min; 40 cycles of 95°C, 30 s; 60°C, 30 s; 72°C, 1 min; final extension 72°C, 2 min. Amplified PCR products were digested with *Hpy* CH4 IV (New England BioLabs, Beverly, MA) at 37°C for 3 h, or *Taq* I (Takara Bio) at 65°C for 3 h and analyzed by electrophoresis. DNA methylation levels were calculated using the formula: estimated methylation degree (%) = $100 \times I^C/(I^C + I^{UC})$, where I^C and I^{UC} represent intensities of digested and undigested bands, respectively. The intensities of bands were determined using ImageJ software provided by the National Institutes of Health (http://rsb.info.nih.gov/ij/). COBRA assay was independently performed twice for all samples. PCR products were cloned into the pGEM T-Easy vector (Promega, Madison, WI), and 10 to 16 clones sequenced to determine DNA methylation status.

Preparation of Porcine Parthenogenetic Embryos

Porcine parthenogenetic embryos were generated as reported previously (Matsunari *et al.*, 2008). Briefly, porcine ovaries were collected at local abattoirs. In vitro maturated oocytes with expanded cumulus cells were treated with 1 mg/ml of hyaluronidase dissolved in Tyrode's lactose medium containing 10 mM HEPES and 0.3% (w/v) polyvinylpyrrolidone (HEPES-TL-PVP), and separated from the cumulus cells by gentle pipetting. Oocytes with evenly granulated ooplasm and an extruded first polar body were selected for subsequent experiments. Oocytes were transferred to an activation solution consisting of 0.3 M mannitol (Nacalai Tesque, Kyoto, Japan), 50 μM $CaCl_2$, 100 μM $MgCl_2$, and 0.01% (w/v) PVA, and activated by applying a single direct current pulse (150 V/mm, 100 μsec) using an electrical pulsing machine (LF201; Nepa Gene, Chiba, Japan). Activated oocytes were cultured and treated with 5 μg/ml cytochalasin B for 3 h to suppress extrusion of the second polar body followed by in vitro culture for up to 4 days to obtain parthenogenetic host embryos at 4 to 8-cell- and morula-stages. In vitro culture of parthenogenetic embryos was performed in porcine zygote medium-5 (PZM-5; Research Institute for the Functional Peptides, Yamagata, Japan) under paraffin oil (Kanto Chemical, Tokyo, Japan) in a humidified atmosphere of 5% CO_2, 5% O_2, and 90% N_2 at 38.5°C.

Production of Aggregated Embryos

Parthenogenetic embryos at 4- to 8-cell (day 3) or morula (day 4) stages were used as host embryos for aggregation of iPSCs. Host 4- to 8-cell embryos or morulae were decompacted by incubation in Ca^{2+}/Mg^{2+}-free Dulbecco phosphate-buffered saline (DPBS; Nissui, Tokyo, Japan) containing 0.1 mM EDTA-2Na and 0.01% (w/v) PVA for 15–20 min, followed by removal of the zona pellucidae by digestion with 0.25% (w/v) pronase in DPBS. Small clumps (~30 cells) of iPSCs were isolated from the feeder layer and kept in a drop of 21 mM Hepes-buffered MEM (Invitrogen) supplemented with 5 mg/ml BSA (Sigma) (MEM-HEPES). Aggregation of iPSC clumps and host embryos was carried out using the micro-well method (Nagy and Rossant, 1993). Each clump of iPSCs was aggregated with host blastomeres isolated from two parthenogenetic embryos at 4- to 8-cell or morula stages.

Some of the parthenogenetic host embryos were aggregated with ICM clumps isolated from parthenogenetic blastocysts on day 6 by immunosurgery as described previously (Nagashima *et al.*, 2004). Isolated ICM cells were labeled with fluorescent carbocyanine dye (DiI, Takara Bio) for 30 min, followed by thorough washing with MEM-HEPES.

Embryos produced by the aggregation method were cultured for 48–72 h in PZM-5. Blastocysts at day 6

were observed by confocal microscopy to analyze the incorporation of the donor cells into the ICM. Images of blastocysts placed in a drop of DPBS containing 5 μg/ml Hoechst 33342 were taken using a confocal fluorescence microscope (FV-1000; Olympus, Tokyo, Japan).

ACKNOWLEDGMENTS

The authors acknowledge Dr. Masaki Nagaya for helpful discussions on this manuscript and Mr. Taisuke Matsuda for technical help.

LITERATURE CITED

Aoi T, Yae K, Nakagawa M, Ichisaka T, Okita K, Takahashi K, Chiba T, Yamanaka S. 2008. Generation of pluripotent stem cells from adult mouse liver and stomach cells. Science 321:699-702.

Brons IG, Smithers LE, Trotter MW, Rugg-Gunn P, Sun B, Chuva de Sousa Lopes SM, Howlett SK, Clarkson A, Ahrlund-Richter L, Pedersen RA, Vallier L. 2007. Derivation of pluripotent epiblast stem cells from mammalian embryos. Nature 448:191-195.

Buehr M, Meek S, Blair K, Yang J, Ure J, Silva J, McLay R, Hall J, Ying QL, Smith A. 2008. Capture of authentic embryonic stem cells from rat blastocysts. Cell 135: 1287-1298.

Chen X, Xu H, Yuan P, Fang F, Huss M, Vega VB, Wong E, Orlov YL, Zhang W, Jiang J, Loh YH, Yeo HC, Yeo ZX, Narang V, Govindarajan KR, Leong B, Shahab A, Ruan Y, Bourque G, Sung WK, Clarke ND, Wei CL, Ng HH. 2008. Integration of external signaling pathways with the core transcriptional network in embryonic stem cells. Cell 133:1106-1117.

Ebert AD, Yu J, Rose FF Jr, Mattis VB, Lorson CL, Thomson JA, Svendsen CN. 2009. Induced pluripotent stem cells from a spinal muscular atrophy patient. Nature 457:277-280.

Ezashi T, Telugu BP, Alexenko AP, Sachdev S, Sinha S, Roberts RM. 2009. Derivation of induced pluripotent stem cells from pig somatic cells. Proc Natl Acad Sci USA 106:10993-10998.

Fujishiro SH, Nakano K, Mizukami Y, Azami T, Arai Y, Matsunari H, Ishino R, Nishimura T, Watanabe M, Abe T, Furukawa Y, Umeyama K, Yamanaka S, Ema M, Nagashima H, Hanazono Y. 2013. Generation of naive-like porcine-induced pluripotent stem cells capable of contributing to embryonic and fetal development. Stem Cells Dev 22:473-482.

Golob JL, Paige SL, Muskheli V, Pabon L, Murry CE. 2008. Chromatin remodeling during mouse and human embryonic stem cell differentiation. Dev Dyn 237:1389-1398.

Hanna J, Markoulaki S, Mitalipova M, Cheng AW, Cassady JP, Staerk J, Carey BW, Lengner CJ, Foreman R, Love J, Gao Q, Kim J, Jaenisch R. 2009. Metastable pluripotent states in NOD-mouse-derived ESCs. Cell Stem Cell 4:513-524.

Hattori N, Nishino K, Ko YG, Hattori N, Ohgane J, Tanaka S, Shiota K. 2004. Epigenetic control of mouse Oct-4 gene expression in embryonic stem cells and trophoblast stem cells. J Biol Chem 279: 17063-17069.

Hayashi K, Ohta H, Kurimoto K, Aramaki S, Saitou M. 2011. Reconstitution of the mouse germ cell specification pathway in culture by pluripotent stem cells. Cell 146:519-532.

Hayashi K, Ogushi S, Kurimoto K, Shimamoto S, Ohta H, Saitou M. 2012. Offspring from oocytes derived from in vitro primordial germ cell-like cells in mice. Science 338:971-975.

Ikegami K, Ohgane J, Tanaka S, Yagi S, Shiota K. 2009. Interplay between DNA methylation, histone modification and chromatin remodeling in stem cells and during development. Int J Dev Biol 53:203-214.

Imaizumi Y, Okada Y, Akamatsu W, Koike M, Kuzumaki N, Hayakawa H, Nihira T, Kobayashi T, Ohyama M, Sato S, Takanashi M, Funayama M, Hirayama A, Soga T, Hishiki T, Suematsu M, Yagi T, Ito D, Kosakai A, Hayashi K, Shouji M, Nakanishi A, Suzuki N, Mizuno Y, Mizushima N, Amagai M, Uchiyama Y, Mochizuki H, Hattori N, Okano H. 2012. Mitochondrial dysfunction associated with increased oxidative stress and alpha-synuclein accumulation in PARK2 iPSC-derived neurons and postmortem brain tissue. Mol Brain 5:35.

Imamura M, Miura K, Iwabuchi K, Ichisaka T, Nakagawa M, Lee J, Kanatsu-Shinohara M, Shinohara T, Yamanaka S. 2006. Transcriptional repression and DNA hypermethylation of a small set of ES cell marker genes in male germline stem cells. BMC Dev Biol 6:34.

Inoue H, Yamanaka S. 2011. The use of induced pluripotent stem cells in drug development. Clin Pharmacol Ther 89:655-661.

Kobayashi T, Yamaguchi T, Hamanaka S, Kato-Itoh M, Yamazaki Y, Ibata M, Sato H, Lee YS, Usui J, Knisely AS, Hirabayashi M, Nakauchi H. 2010. Generation of rat pancreas in mouse by interspecific blastocyst injection of pluripotent stem cells. Cell 142:787-799.

Li P, Tong C, Mehrian-Shai R, Jia L, Wu N, Yan Y, Maxson RE, Schulze EN, Song H, Hsieh CL, Pera MF, Ying QL. 2008. Germline competent embryonic stem cells derived from rat blastocysts. Cell 135:1299-1310.

Lieb JD, Beck S, Bulyk ML, Farnham P, Hattori N, Henikoff S, Liu XS, Okumura K, Shiota K, Ushijima T, Greally JM. 2006. Applying whole-genome studies of epigenetic regulation to study human disease. Cytogenet Genome Res 114:1-15.

Lunney JK. 2007. Advances in swine biomedical model genomics. Int J Biol Sci 3:179-184.

Matsunari H, Onodera M, Tada N, Mochizuki H, Karasawa S, Haruyama E, Nakayama N, Saito H, Ueno S, Kurome M, Miyawaki A, Nagashima H. 2008. Transgenic-cloned pigs systemically expressing red fluorescent protein, Kusabira-Orange. Cloning Stem Cells 10:313-323.

Meissner A, Mikkelsen TS, Gu H, Wernig M, Hanna J, Sivachenko A, Zhang X, Bernstein BE, Nusbaum C, Jaffe DB, Gnirke A, Jaenisch R, Lander ES. 2008. Genome-scale DNA methylation maps of pluripotent and differentiated cells. Nature 454:766-770.

Montserrat N, Bahima EG, Batlle L, Häfner S, Rodrigues AM, González F, Izpisúa Belmonte JC. 2011. Generation of pig iPS cells: A model for cell therapy. J Cardiovasc Transl Res 4:121-130.

Nagashima H, Giannakis C, Ashman RJ, Nottle MB. 2004. Sex differentiation and germ cell production in chimeric pigs produced by inner cell mass injection into blastocysts. Biol Reprod 70:702-707.

Nagy A, Rossant J. 1993. Production of completely ES cell-derived fetuses. In: Joyner AL, editor. Gene targeting: a practical approch. UK: IRL Press. p 147-179.

Niwa H, Miyazaki J, Smith AG. 2000. Quantitative expression of Oct-3/4 defines differentiation, dedifferentiation or self-renewal of ES cells. Nat Genet 24:372-376.

Okita K, Ichisaka T, Yamanaka S. 2007. Generation of germline-competent induced pluripotent stem cells. Nature 448:313-317.

Okita K, Yamanaka S. 2011. Induced pluripotent stem cells: opportunities and challenges. Philos Trans R Soc Lond B Biol Sci 366:2198-2207.

Petters RM. 1994. Transgenic livestock as genetic models of human disease. Reprod Fertil Dev 6:643-645.

Prather RS, Hawley RJ, Carter DB, Lai L, Greenstein JL. 2003. Transgenic swine for biomedicine and agriculture. Theriogenology 59:115-123.

Rodríguez A, Allegrucci C, Alberio R. 2012. Modulation of pluripotency in the porcine embryo and iPS cells. PLoS One 7:e49079.

Sakaki-Yumoto M, Kobayashi C, Sato A, Fujimura S, Matsumoto Y, Takasato M, Kodama T, Aburatani H, Asashima M, Yoshida N, Nishinakamura R. 2006. The murine homolog of SALL4, a causative gene in Okihiro syndrome, is essential for embryonic stem cell proliferation, and cooperates with Sall1 in anorectal, heart, brain and kidney development. Development 133:3005-3013.

Sakamoto H, Suzuki M, Abe T, Hosoyama T, Himeno E, Tanaka S, Greally JM, Hattori N, Yagi S, Shiota K. 2007. Cell type-specific methylation profiles occurring disproportionately in CpG-less regions that delineate developmental similarity. Genes Cells 10:1123-1132.

Sato S, Yagi S, Arai Y, Hirabayashi K, Hattori N, Iwatani M, Okita K, Ohgane J, Tanaka S, Wakayama T, Yamanaka S, Shiota K. 2010. Genome-wide DNA methylation profile of tissue-dependent and differentially methylated regions (T-DMRs) residing in mouse pluripotent stem cells. Genes Cells 15:607-618.

Shiota K. 2004. DNA methylation profiles of CpG islands for cellular differentiation and development in mammals. Cytogenet Genome Res 105:325-334.

Shiota K, Kogo Y, Ohgane J, Imamura T, Urano A, Nishino K, Tanaka S, Hattori N. 2002. Epigenetic marks by DNA methylation specific to stem, germ and somatic cells in mice. Genes Cells 7:961-969.

Takahashi K, Tanabe K, Ohnuki M, Narita M, Ichisaka T, Tomoda K, Yamanaka S. 2007. Induction of pluripotent stem cells from adult human fibroblasts by defined factors. Cell 131:861-872.

Takahashi K, Yamanaka S. 2006. Induction of pluripotent stem cells from mouse embryonic and adult fibroblast cultures by defined factors. Cell 126:663-676.

Tesar PJ, Chenoweth JG, Brook FA, Davies TJ, Evans EP, Mack DL, Gardner RL, McKay RD. 2007. New cell lines from mouse epiblast share defining features with human embryonic stem cells. Nature 448:196-199.

Tsubooka N, Ichisaka T, Okita K, Takahashi K, Nakagawa M, Yamanaka S. 2009. Roles of Sall4 in the generation of pluripotent stem cells from blastocysts and fibroblasts. Genes Cells 14:683-694.

Usui J, Kobayashi T, Yamaguchi T, Knisely AS, Nishinakamura R, Nakauchi H. 2012. Generation of kidney from pluripotent stem cells via blastocyst complementation. Am J Pathol 180:2417-2426.

van der Spoel TI, Jansen of Lorkeers SJ, Agostoni P, van Belle E, Gyöngyösi M, Sluijter JP, Cramer MJ, Doevendans PA, Chamuleau SA. 2011. Human relevance of pre-clinical studies in stem cell therapy: systematic review and meta-analysis of large animal models of ischaemic heart disease. Cardiovasc Res 91:649-658.

West FD, Terlouw SL, Kwon DJ, Mumaw JL, Dhara SK, Hasneen K, Dobrinsky JR, Stice SL. 2010. Porcine induced pluripotent stem cells produce chimeric offspring. Stem Cells Dev 8:1211-1220.

West FD, Uhl EW, Liu Y, Stowe H, Lu Y, Yu P, Gallegos-Cardenas A, Pratt SL, Stice SL. 2011. Chimeric pigs produced from induced pluripotent stem cells demonstrate germline transmission and no evidence of tumor formation in young pigs. Stem Cells 10:1640-1643.

Wu Z, Chen J, Ren J, Bao L, Liao J, Cui C, Rao L, Li H, Gu Y, Dai H, Zhu H, Teng X, Cheng L, Xiao L. 2009. Generation of pig induced pluripotent stem cells with a drug-inducible system. J Mol Cell Biol 1:46-54.

Xu J, Pope SD, Jazirehi AR, Attema JL, Papathanasiou P, Watts JA, Zaret KS, Weissman IL, Smale ST. 2007.

Pioneer factor interactions and unmethylated CpG dinucleotides mark silent tissue-specific enhancers in embryonic stem cells. Proc Natl Acad Sci USA 104:12377–12382.

Yagi S, Hirabayashi K, Sato S, Li W, Takahashi Y, Hirakawa T, Wu G, Hattori N, Hattori N, Ohgane J, Tanaka S, Liu XS, Shiota K. 2008. DNA methylation profile of tissue-dependent and differentially methylated regions (T-DMRs) in mouse promoter regions demonstrating tissue-specific gene expression. Genome Res 18:1969–1978.

Xiong Z, Laird PW. 1997. COBRA: a sensitive and quantitative DNA methylation assay. Nucleic Acids Res 25: 2532–2534.

Zhao MT, Prather RS. 2011. The multi-potentiality of skin-derived stem cells in pigs. Theriogenology 75: 1372–1380.

Zhou L, Wang W, Liu Y, Fernandez de Castro J, Ezashi T, Telugu BP, Roberts RM, Kaplan HJ, Dean DC. 2011. Differentiation of induced pluripotent stem cells of swine into rod photoreceptors and their integration into the retina. Stem Cells 29:972–980.

Maehara et al. BMC Biotechnology 2013, 13:58
http://www.biomedcentral.com/1472-6750/13/58

BMC Biotechnology

METHODOLOGY ARTICLE Open Access

Development of a novel vitrification method for chondrocyte sheets

Miki Maehara[1,2], Masato Sato[3], Masahito Watanabe[1,2], Hitomi Matsunari[1,2], Mami Kokubo[3], Takahiro Kanai[1], Michio Sato[4], Kazuaki Matsumura[5], Suong-Hyu Hyon[6], Munetaka Yokoyama[3], Joji Mochida[3] and Hiroshi Nagashima[1,2*]

Abstract

Background: There is considerable interest in using cell sheets for the treatment of various lesions as part of regenerative medicine therapy. Cell sheets can be prepared in temperature-responsive culture dishes and applied to injured tissue. For example, cartilage-derived cell sheets are currently under preclinical testing for use in treatment of knee cartilage injuries. The additional use of cryopreservation technology could increase the range and practicality of cell sheet therapies. To date, however, cryopreservation of cell sheets has proved impractical.

Results: Here we have developed a novel and effective method for cryopreserving fragile chondrocyte sheets. We modified the vitrification method previously developed for cryopreservation of mammalian embryos to vitrify a cell sheet through use of a minimum volume of vitrification solution containing 20% dimethyl sulfoxide, 20% ethylene glycol, 0.5 M sucrose, and 10% carboxylated poly-L-lysine. The principal feature of our method is the coating of the cell sheet with a viscous vitrification solution containing permeable and non-permeable cryoprotectants prior to vitrification in liquid nitrogen vapor. This method prevented fracturing of the fragile cell sheet even after vitrification and rewarming. Both the macro- and microstructures of the vitrified cell sheets were maintained without damage or loss of major components. Cell survival in the vitrified sheets was comparable to that in non-vitrified samples.

Conclusions: We have shown here that it is feasible to vitrify chondrocyte cell sheets and that these sheets retain their normal characteristics upon thawing. The availability of a practical cryopreservation method should make a significant contribution to the effectiveness and range of applications of cell sheet therapy.

Keywords: Cell sheet therapy, Chondrocyte sheet, Vitrification, Cryopreservation, Cartilage repair

Background

The use of cell sheets is being actively investigated in the field of regenerative medicine as a potential treatment for various lesions [1,2]. For example, Okano et al. developed a method of preparing various types of cell sheets using temperature-responsive culture dishes [3]; additionally, cell sheets derived from corneal epithelia [4], skin [5], oral mucosal epithelia [6], bladder epithelia [7], myocardial cells [8,9], periodontal ligaments [10], and cartilage [11,12] are currently under investigation in preclinical studies or clinical applications [13-15].

We have been investigating the use of chondrocyte-derived cell sheets for treatment of knee cartilage injuries [11,12,16-18]. Cell sheets can be used as autografts or allografts. In a clinical setting, the preparation of autologous cell sheets involves a defined period of time for culture of the cells. Thus, the timing of transplantation has to be arranged with regard to both the needs of the patient and the condition of the cultured cell sheet. Cryopreservation of cell sheets would simplify the coordination of transplantation timing and would also allow repeated treatments for a single patient. In addition, development of robust cryopreservation methods and distribution protocols would need to be established to facilitate allograft-based cell sheet therapy. There is little doubt that cryopreservation of cell sheets would provide significant benefits to clinical applications of cell sheet therapies.

* Correspondence: hnagas@isc.meiji.ac.jp
[1]Laboratory of Developmental Engineering, School of Agriculture, Meiji University, 1-1-1 Higashimita, Tama, Kawasaki, Japan
[2]Meiji University International Institute for Bio-Resource Research (MUIIBR), 1-1-1 Higashimita, Tama, Kawasaki, Japan
Full list of author information is available at the end of the article

Cell sheet therapy involves covering a tissue lesion with a membranous sheet [11,19,20]. Therefore, an indispensable prerequisite of a cryopreservation method is to maintain the integrity of the membranous structure of the cell sheet. However, achieving this has been challenging and although the viability of the cells comprising the sheets can be maintained, damage to the integrity of the sheet often occurs [21]. To date, no practical cryopreservation method has been developed for cell sheets that have been generated in temperature-responsive culture dishes.

Recent developments in vitrification methods have allowed practical cryopreservation of early stage embryos of many mammalian species, including humans [22,23]. Embryos are highly susceptible to damage by various aspects of cryopreservation, including the toxicity of the cryoprotectant (CPA), osmotic shock, and temperature shock [23,24], which makes their successful cryopreservation more difficult compared to somatic cells. Furthermore, embryos of some mammalian species such as pigs [25-28] are especially sensitive to low temperatures. However, the latest vitrification methods have enabled very high post-cryopreservation survival rates for mammalian embryos of a wide range of species, derivations or backgrounds [23,29,30]. The basic principle of the latest high-performance method involves vitrifying embryos with a very small amount of vitrification solution, a process termed the minimum volume cooling (MVC)-vitrification method [29-32]. The MVC-vitrification method is effective at stabilizing the vitreous status of the solution during vitrification and rewarming, and thereby achieves a high rate of survival of embryos.

In light of the success achieved in embryos, we decided to apply the basic principles of the MVC-vitrification method for cryopreservation of chondrocyte sheets. We successfully developed a coating method by which a cell sheet could be vitrified using a minimum amount of solution. This report describes the development of an effective vitrification method that does not impair either the macro- or microstructures of cell sheets, and thereby possesses significant potential for applications related to clinical cell sheet therapy.

Methods

Chemicals

All chemicals were purchased from Sigma-Aldrich Chemical Co. (MO, USA), unless otherwise indicated.

Preparation of rabbit chondrocyte sheets

The study was conducted using commercially available primary cultured cells (Primary Cell, Hokkaido, Japan) derived from the knee cartilage of a Japanese white rabbit. The cells were plated onto temperature-responsive culture dishes (UpCell, diameter: 35 mm; CellSeed, Tokyo, Japan) [3] at a density of 5.0×10^4 to 1.0×10^5 cells/dish and cultured in RPMI-1640 medium (11875; GIBCO, Life Technologies Corporation, CA, USA) supplemented with 10% fetal bovine serum (FBS; 171012, Nichirei Biosciences, Tokyo, Japan) at 37°C in a humidified atmosphere of 5% CO_2 in air. The medium in each dish was replaced with the same medium supplemented with 100 μM L-ascorbic acid (A4544; Wako Pure Chemical Industries, Osaka, Japan) when the cells reached confluence. The cells formed a single thin layer after 2 weeks of plating, at which time the UpCell dishes were placed at 25°C for 30 min to promote detachment of the cell sheet from the bottom surface of the dish [11]. The cell sheet was then removed from the dish using a cell shifter (CellSeed). Three cell sheets were layered together to form a triple-layered sheet, and this sheet was further cultured for 1 week in the UpCell dish.

Vitrification solutions

The vitrification solution developed for cryopreserving mammalian embryos [22,32] was used after slight modifications.

Hepes (20 mM) buffered Tissue Culture Medium-199 (Nissui Pharmaceutical, Tokyo, Japan) supplemented with 20% calf serum (12133C; SAFC Biosciences, KS, USA) was used as the basal solution. Dimethyl sulfoxide (DMSO) and ethylene glycol (EG) were used as permeable CPAs. Sucrose was used as a non-permeable CPA for all vitrification experiments. In some experimental groups, carboxylated poly-L-lysine (COOH-PLL) [33] was also added as a supplemental non-permeable CPA.

An equilibration solution (ES) consisting of 10% (v/v) DMSO and 10% (v/v) EG in the basal solution and a vitrification solution (VS) containing 20% (v/v) DMSO, 20% (v/v) EG, and 0.5 M sucrose were prepared. The effect of supplementation of the VS with 10% (w/v) COOH-PLL was examined in some of the experimental groups. A rewarming solution (RS) and a dilution solution (DS) containing 1 M and 0.5 M sucrose, respectively, were prepared and the basal solution was used as the washing solution (WS).

The VS was used at ice temperature (on crushed ice), and pre-warmed RS at 38°C was used to devitrify (rewarm) the vitrified cell sheet. All other solutions were used at room temperature (24-27°C).

Vitrification procedures

Coating method

The development of the coating method for the chondrocyte sheets was guided by the MVC concept [31], which has been shown to be effective for the vitrification of mammalian embryos. The method used here involves vitrification of a cell sheet; this is achieved by treating a cell sheet with ES and VS and then applying a thin coat of VS containing permeable and non-permeable CPAs.

This technique enables vitrification of the cell sheet with the minimum amount of vitrification solution (Figure 1).

First, a triple-layered cell sheet was peeled from the UpCell surface using a cell shifter and forceps, and immersed in 5 ml of ES in a 60 mm dish (Iwaki 3010–060, AGC Techno Glass, Shizuoka, Japan) for 5 min for pre-equilibration. Then, the cell sheet was transferred to the same solution in a fresh dish for 20 min (equilibration). After equilibration, the cell sheet was transferred to VS using forceps for 5 min (VS pre-treatment), and then transferred to fresh VS in another dish for 15 min for dehydration and the permeation of the permeable CPAs. VS containing COOH-PLL and unmodified VS were compared. After VS treatment, the cell sheet was carefully placed on a stainless steel mesh (30 mm) using forceps (Figure 2A). The cell sheet on the mesh was held 1 cm above the surface of liquid nitrogen (LN) in a 1 L Styrofoam bath and was vitrified by a 20 min exposure to the LN vapor (−140°C) (Figure 2B). We observed that vitrification of the cell sheet was completed within the first 5 min (Figure 2C). The use of LN vapor was adopted after preliminary tests demonstrated that the cell sheet fractured when it was directly immersed in LN.

To rewarm a vitrified sheet, the mesh holding the sheet was placed directly onto an electric heating plate (HP-4530; ASONE Corporation, Osaka, Japan) at 38°C for 90 sec (Figure 2D). After the sheet had completely thawed, the mesh holding the sheet was slowly placed into 10 ml of RS in a 60 mm dish and was gently removed from the mesh using forceps (Figure 2E). At this stage, the recovered sheet was checked for cracks. The CPAs were diluted and removed in a stepwise manner. Briefly, the cell sheet was held in RS for 1 min and then transferred into 5 ml of DS using forceps for 3 min. Then, the cell sheet was transferred twice into 5 ml of WS. The cell sheet was gently shaken several times in each solution to help diffusion of the CPAs.

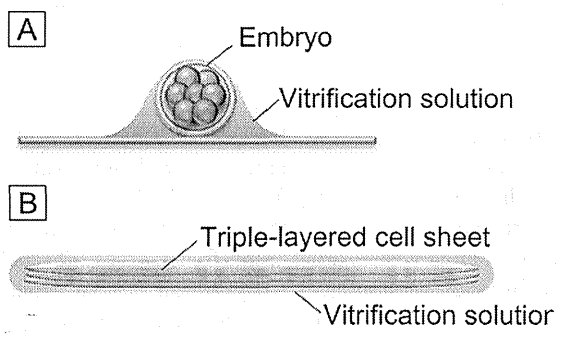

Figure 1 The minimum volume cooling concept applied to vitrification of an embryo and a cell sheet. A: The protocol of embryo vitrification using the minimum volume cooling (MVC) concept; the embryo is vitrified in a minimum volume of vitrification solution on a plastic or metal plate with high thermal conductivity [22,32]. **B**: For cryopreservation of triple-layered rabbit chondrocyte sheets, we developed a coating method in which the cultured cell sheet is thinly coated with a viscous vitrification solution containing permeable and non-permeable cryoprotectants. This enables the cell sheet to be vitrified in a minimum amount of vitrification solution in accordance with the MVC concept.

Envelope method

A cell sheet pre-treated with ES and VS as described above in the coating method, was placed onto a 5 × 10 cm rectangular piece of polyvinylidene chloride kitchen wrap (Kureha Corporation, Tokyo, Japan) using forceps. Then, the wrapping film was folded to enclose the cell sheet (Figure 2F). The wrapped sheet was held 1 cm above the surface of LN and vitrified by exposure to the vapor for 20 min (Figure 2G). Vitrification of the cell sheet was observed within the first 5 min (Figure 2H). As the presence of COOH-PLL in the VS was found to be essential for maintaining the structure of the vitrified sheet in the development of the coating method described above, VS containing COOH-PLL was used for the envelope method.

To rewarm the vitrified sheet, the cell sheet envelope was placed directly onto a heating plate at 38°C for 90 sec (Figure 2I). When the sheet had completely thawed, the wrapping film was slowly opened and the sheet was transferred into RS using forceps (Figure 2J). The recovered sheet was checked for cracks, and the CPAs were diluted, removed, and washed as described above for the coating method.

Dish method

In order to evaluate the effect of VS volume on cell sheet vitrification, a sheet was immersed in 2 ml of VS, a considerably larger volume than used in the coating or envelope methods.

A preliminary study revealed the formation of many cracks and ice crystals when the vitrification/rewarming procedure was performed using 2 ml of VS in a 35 mm plastic dish (Additional file 1: Figure S1A). However, ice crystal and crack formation was significantly reduced when the VS contained 10% COOH-PLL (Additional file 1: Figure S1B). Therefore, the dish method was performed using VS containing COOH-PLL.

A cell sheet was pretreated with ES and VS in the same manner as in the coating and envelope methods, placed in 2 ml of VS in a 35 mm dish (Nunc 150318, Thermo Fisher Scientific, Kanagawa, Japan) for 15 min for further CPA permeation and dehydration (Figure 2K). The dish was held 1 cm above the surface of LN for 20 min (Figure 2L) to induce solidification of the VS containing the sheet (Figure 2M).

To rewarm the vitrified sheet, the dish was allowed to stand for 3 min on a heating plate at 38°C (Figure 2N).

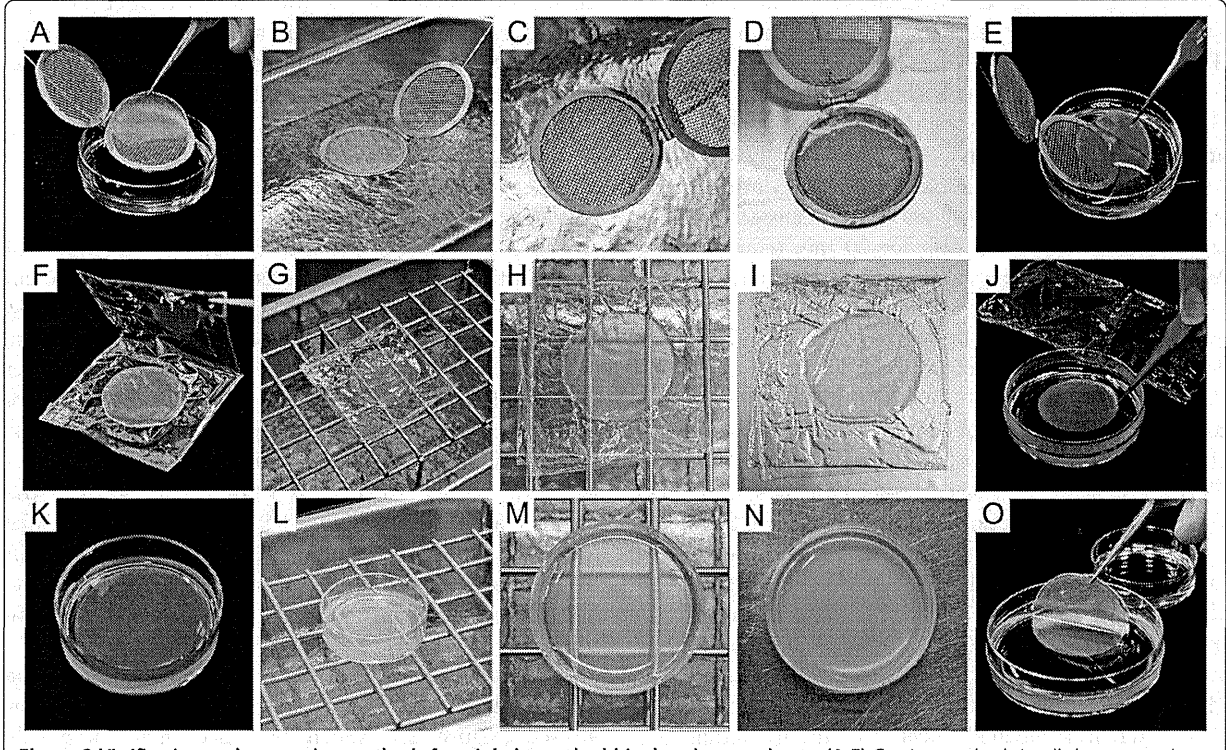

Figure 2 Vitrification and rewarming methods for triple-layered rabbit chondrocyte sheets. (A-E) Coating method. A cell sheet treated with ES and VS is placed on a stainless mesh using forceps **(A)** and exposed to liquid nitrogen (LN) vapor for vitrification **(B)**. **(C)** A cell sheet vitrified on mesh. Note the transparency of the vitrified sheet. For rewarming, the vitrified sheet on a mesh device is placed on a heating plate for thawing **(D)** and then transferred to RS using forceps **(E)**. **(F-J)** Wrapping film method. An ES- and VS-treated cell sheet was wrapped in an envelope of polyvinylidene chloride film **(F)** and exposed to LN vapor for vitrification **(G)**. **(H)** A cell sheet vitrified in wrapping film. Note that the cell sheet is transparent when it solidifies. For rewarming, the sheet vitrified in the wrapping film is placed on a heating plate **(I)**, followed by transfer into RS **(J)**. **(K-O)** Dish method. A cell sheet pretreated with ES and VS is placed in 2 ml VS **(K)** and exposed to LN vapor for vitrification **(L)**. **(M)** A cell sheet solidified with VS in a dish. Note the transparency of the vitrified solution and the lack of any cracks. **(N)** A dish containing a cell sheet on a heating plate for rewarming. The opacity of the solution indicates that ice crystals have formed during the warming process. The thawed cell sheet is then transferred into RS using forceps **(O)**.

After the complete melting of the VS in the dish, the cell sheet was transferred into RS using forceps (Figure 2O) and checked for visible damage (cracks). The CPAs were diluted, removed, and washed in the same manner as in the coating method.

Survival of the cells in the vitrified cell sheet

A vitrified cell sheet recovered after rewarming, rehydration and removal of CPAs was transferred into Dulbecco's phosphate-buffered saline (D-PBS; 10 ml) for washing. The cell sheet was cut into 1–2 mm^2 pieces with ophthalmic scissors, and the pieces were incubated in RPMI-1640 medium containing 2 mg/ml collagenase II (17101; GIBCO) at 37°C for 40–50 min to isolate the cells. The suspension of isolated cells was centrifuged at 1,000 rpm for 5 min, and the precipitated cells were resuspended in RPMI-1640 medium (22400; GIBCO) and their viability was determined after trypan blue staining (viability (%) = live cells/live and dead cells × 100).

Electron microscopy

Triple-layered chondrocyte sheets were soaked in 0.1 mol/l D-PBS containing 2% glutaraldehyde for 2 h, then fixed in 2% osmium tetroxide solution for 1 h, and then dehydrated through an ethanol series (50, 70, 80, 90, 95, and 100%). Next, the ethanol was replaced by 100% *tert*-butyl alcohol, and the samples were dried using freeze dryer (ES-2030; Hitachi High-Technologies Corporation, Tokyo, Japan). The dried specimens were sputter-coated with osmium and affixed to an adhesive interface for observation with a scanning electron microscope (JSM-6700 F; JEOL, Tokyo, Japan). The top surfaces of the cell sheets were observed at magnifications ranging from × 300 to × 2,000.

Histological examination and immunohistochemical staining

Triple-layered cell sheets were harvested after culture or cryopreservation and fixed in 4% paraformaldehyde solution for 1 week. The specimens were embedded in

paraffin and sectioned, and the sections were placed on glass slides. After deparaffinization and rehydration, the sections were stained for proteoglycan with 0.1% Safranin-O or immunostained with type II collagen antibody. For immunohistochemistry, the slides were incubated with a diluted primary anti-human type II collagen antibody (F-57: Daiichi Fine Chemical, Toyama, Japan) for 16 h at 4°C, followed by incubation with the EnVision + Mouse/HRP secondary antibody (K4000: DAKO, Glostrup, Denmark) for 1 h at room temperature. Finally, the sections were stained with diaminobenzidine (K3466: DAKO) and counterstained with hematoxylin. Coverslips were mounted onto the slides and sealed with nail polish. The slides were then examined under a microscope and images were captured (Biozero BZ-8000, KEYENCE, Osaka, Japan).

Statistical analysis

Statistical analyses were performed using IBM SPSS Statistics 20.0 software (IBM Corporation, NY, USA). The proportional data were subjected to arcsine transformation and evaluated by one-way analysis of variance (ANOVA) followed by multiple comparisons using Tukey's test. The level of significance was set at p values < 0.05.

Results and discussion

Maintenance of cell sheet structure and cell viability after vitrification

Ten cell sheets were vitrified using the coating method in the presence of 10% COOH-PLL (Table 1). After rewarming, all the recovered sheets (100%) showed no visible damage and had same appearance as non-vitrified cell sheets (Figure 3A, B). Eight sheets were vitrified using the coating method in the absence of COOH-PLL (Table 1); only one of the recovered sheets (12.5%) did not have visible damage, all of the remainder exhibited cracks (Figure 3C). Cell viability in the vitrified cell sheets did not differ between protocols with or without COOH-PLL (92.1% vs. 91.9%); the rates of cell viability were comparable to that of the non-vitrified control (94.6%).

These results clearly showed that vitrification by the coating method in the presence of COOH-PLL as a supplemental non-permeable CPA was capable of preserving the membranous structure of the cell sheet with a high survival rate for the constituent cells. To the best of our knowledge, our results represent the first successful vitrification of cell sheets grown in temperature-responsive dishes. In this study, we vitrified cell sheets in LN vapor rather than by direct immersion in the LN. This also had a critical influence on the maintenance of the membranous structure of the cell sheet during vitrification. In preliminary experiments, all of the cell sheets cracked, even in the presence of COOH-PLL, when they were vitrified by direct immersion in LN. Possibly, the direct immersion approach might have had a more drastic impact on membrane integrity than the vapor and, thereby, impaired cell sheet structure.

Since the coating method proved successful for vitrification of cell sheets, we examined whether cell sheets enveloped in a thin film could also be vitrified successfully. Seven cell sheets were placed into film envelopes, vitrified and rewarmed (Table 1). All the sheets (100%) were recovered without visible damage (Figure 3D). However, cell viability (86.8%) was slightly lower compared to that in the coating method ($p < 0.05$).

For use in clinical applications, it would be preferable if vitrified cell sheets could be stored and distributed in hygienic coverings. Our results demonstrated that a cell sheet enveloped in a thin film with a minimum volume of VS could be successfully vitrified. However, wrapping a cell sheet with a film might influence the optimal cooling and rewarming rates during vitrification and rewarming processes. As cooling and warming rates have a crucial influence on the viability of vitrified cells [34,35], it will be important to identify robust film materials that have high thermal conductivity and are protective against invasive pathogens, as well as improving cooling and rewarming methods.

We also examined the influence of the volume of vitrification solution on the morphology and survival of cell sheets. Seven cell sheets were vitrified using the dish method (Table 1) that involves a substantially greater

Table 1 Structural maintenance and cell viability after vitrification of triple-layered rabbit chondrocyte sheets

Vitrification method	Presence of COOH-PLL in VS*	No. of cell sheets recovered without fracture / No. of cell sheets examined (%)	Cell viability (mean ± SEM)
Non-vitrified control		8/8 (100)	94.6 ± 0.5^{a}
Coating	+	10/10 (100)	92.1 ± 0.9^{a}
	-	1/8 (12.5)	91.9 ± 0.7^{a}
Envelope	+	7/7 (100)	86.8 ± 0.7^{b}
Dish	+	7/7 (100)	77.6 ± 3.15^{c}

[a-c]Values with different superscript differ significantly ($p < 0.05$).
*VS: Vitrification Solution.

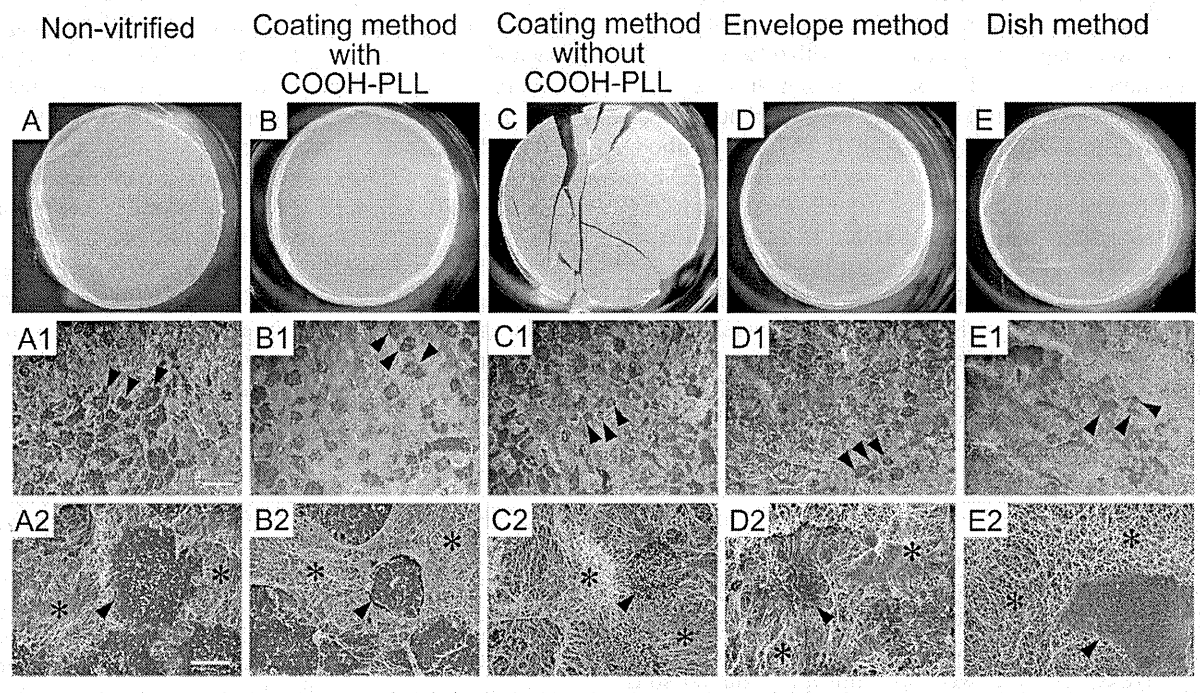

Figure 3 The macro- and microstructures of triple-layered rabbit chondrocyte sheets after vitrification. A-E: Morphological appearance of chondrocyte sheets after vitrification and rewarming. **A1-E2**: Scanning electron microscopic images of the surfaces of cell sheets recovered after vitrification and rewarming. **A1-E1**: ×300, Scale bar = 50 μm; **A2-E2**: ×2,000, Scale bar = 10 μm. The surfaces **(A1-E2)** are irregular, featuring pavement-like cell populations (arrowheads in **A1-E1** indicate representative three cells) and well-developed extracellular matrices with a dense fibrous structure (*). The microstructures of cell sheets vitrified by any of the methods described in this report were similar to those of the non-vitrified control sample.

volume of VS than the coating and envelope methods. VS containing COOH-PLL was used because a preliminary experiment revealed that its presence was essential to ensure crack-free vitrification using the dish method (Additional file 1: Figure S1). All of the 7 sheets (100%) that were vitrified were recovered without any cracks (Figure 3E). However, cell viability after vitrification was 77.6%, which was significantly lower than that observed following vitrification with the coating or envelope methods ($p < 0.05$).

High levels of viability can be achieved by minimizing the volume of the solution used for vitrification of mammalian embryos [31]. In contrast, the vitreous state becomes unstable when larger solution volumes are employed: more cracks tend to occur during the solidification of the solution and more ice crystals form upon rewarming. Our results demonstrated that addition of COOH-PLL as a non-permeable CPA was effective in stabilizing the vitrified state of the solution. However, even when the VS contained COOH-PLL, cell viability was reduced slightly with the dish method. The decrease might be attributed to the slower cooling and warming rates and/or ice crystal formation during rewarming. We observed that the VS appeared opaque for a moment during the rewarming process in the dish method, suggesting the occurrence of ice crystal formation.

Scanning electron microscopic images of the surface of vitrified cell sheets

The microstructures of the cell sheets vitrified in the four experimental groups were compared to those of the non-vitrified sample (Figure 3). Although slight differences were observed among individual sheets, overall, the cell sheets retained their basic structure of pavement-like cells (Figure 3A1-E2) distributed within well-developed extracellular matrices (Figure 3A2-E2). The sheet surfaces were irregular, featuring well-developed extracellular matrices with dense fibrous structures (Figure 3A1-E2).

The microstructures of cell sheets were maintained in the vitrified samples of all the experimental groups under the same conditions as the non-vitrified control groups. The sheets that developed cracks during vitrification with the coating method in the absence of COOH-PLL showed no microstructural abnormalities (Figure 3C1, C2), suggesting that the fracturing of the sheet structure did not affect the microstructure. The sheets vitrified by the envelope method (Figure 3D1, D2) and the dish method (Figure 3E1, E2), where cell viabilities were slightly

decreased, also exhibited no microstructural abnormalities. These results indicate that the microstructure of the vitrified cell sheet, including the extracellular matrix, were well maintained even after vitrification and rewarming under suboptimal conditions.

Histological and immunohistochemical examination of vitrified cell sheets

Cell sheets vitrified with the coating and envelope methods in the presence of COOH-PLL were histochemically and immunohistochemically examined to investigate the distribution of the major components of cartilage, i.e. proteoglycan and type II collagen. In the non-vitrified control (Figure 4A) and the vitrified cell sheet, strong Safranin-O staining was exhibited (coating method: Figure 4C, envelope method: Figure 4E). These results showed that acidic proteoglycan were, in general, densely and evenly distributed throughout the chondrocyte sheet and this distribution pattern was maintained after vitrification in the coating and envelope methods.

The vitrified samples also exhibited large amounts of type II collagen (Figure 4D, F) in a similar manner as in the non-vitrified control (Figure 4B). Overall, these data showed that the extracellular matrix of the vitrified cell sheets had been maintained in both the coating and envelope methods.

Significance of maintaining membranous structure in chondrocyte sheet cryopreservation

In the conventional slow-freezing method, cultured cell sheets are frozen in the presence of a relatively low concentration of a CPA [21]. Thus, extra- and intracellular ice crystal formation is inevitable during freezing, which destroys the cell sheet structure and decreases cell viability [21]. In contrast, with the vitrification method, a solution containing a high concentration of a CPA is rapidly cooled to achieve the transition from the liquid phase to the solid phase (amorphous) without ice crystal formation [36]. Therefore, cell sheets could be sealed in a glassy state that maintained their macro- and microstructures and also allowed high cell viability.

In cell sheet therapy, cytokines and growth factors produced by the cell sheet play an important role in healing damaged tissues [11,19,20]. We found that the formation of a chondrocyte sheet structure enhanced transforming growth factor-β secretion from the cells [37], which implies that maintaining the membranous structure after cryopreservation is a prerequisite for

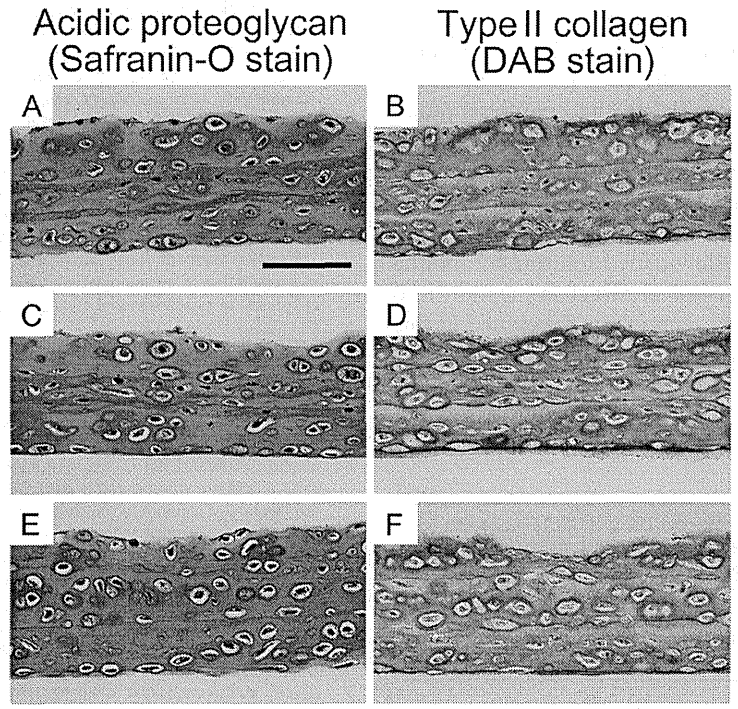

Figure 4 Histological and immunohistochemical examination of triple-layered rabbit chondrocyte sheets. Staining for proteoglycan **(A, C, E)** and type II collagen **(B, D, F)** on cross-sections of cell sheets recovered after vitrification and rewarming. **A, B**: Non-vitrified control cell sheet exhibiting large amounts of proteoglycan and type II collagen in the extracellular matrix. **C, D**: Cell sheet vitrified with the coating method using VS containing COOH-PLL; the sheet exhibits a normal extracellular matrix. **E, F**: Cell sheets vitrified by the envelope method. The extracellular matrix exhibits no difference to samples from control and coating method groups. (Scale bar = 100 μm).

function. Therefore, in the present study, we focused on both the maintenance of sheet structures and of cell viability after vitrification. Thus, our study provides the first demonstration that cryopreservation of cultured chondrocyte sheets with a fragile membranous structure can be achieved using a vitrification method developed on the basis of the MVC concept. Biochemical functions such as cytokine production by the vitrified chondrocyte sheets has yet to be analyzed. Additionally, transplantation experiments using vitrified cell sheets are under consideration.

In our preliminary study, we could successfully vitrify cell sheets with more fragile characteristics including human chondrocyte sheets. It is, therefore, likely that the vitrification method developed in the present study can be applied to different types of cell sheet other than the triple layered rabbit chondrocyte sheets. In application of the vitrification technology to human therapies, toxicity of CPAs to human cells needs to be verified.

Conclusions

In this study, we demonstrate that the vitrification method developed here facilitated the cryopreservation of a chondrocyte sheet while maintaining its macro- and microstructures and allowing a high rate of viability of the constituent cells. The coating method, where the cell sheet was vitrified with a minimum volume of VS in the presence of COOH-PLL, effectively prevented structural damage due to vitrification. Here, we propose three basic principles essential to the cryopreservation of chondrocyte sheets: (i) minimizing the volume of the vitrification solution by using the coating method, (ii) stabilizing the vitreous state via the addition of COOH-PLL as a non-permeable CPA, and (iii) preventing the occurrence of cracks in the vitrified solution by cooling samples in LN vapor instead of direct immersion into LN. The cryopreservation technology developed in this study will play a pivotal role in clinical applications of cell sheet-based therapies.

Additional file

Additional file 1: Figure S1. Protective effect of COOH-PLL against fracture of vitrified solution. COOH-PLL-free (A) and COOH-PLL-containing (B) solutions in the process of rewarming after vitrification in liquid nitrogen vapor. Note the occurrence of many cracks in the COOH-PLL-free solution (A), while the COOH-PLL-containing solution is free of cracks (B). The opacity of the solution in B indicates that ice crystals formed during the warming process.

Abbreviations

COOH-PLL: Carboxylated poly-L-lysine.

Competing interests

The authors declare that they have no competing interests.

Authors' contributions

HN conceived and designed the experiments and wrote the manuscript. MM performed the experiments and wrote the manuscript together with HN. MW wrote the manuscript together with HN. TK and HM performed the experiments. MS (Michio Sato) scanned electron microscopic images. MY, MK prepared chondrocyte cell sheets. KM and HSH prepared COOH-PLL. MS (Masato Sato) and JM helped to draft the manuscript. All authors read and approved the final manuscript.

Acknowledgements

This work was supported by Health and Labour Science Research Grants-Research on Regenerative Medicine for Clinical Application and Meiji University International Institute for Bio-Resource Research (MUIIBR).

Author details

[1]Laboratory of Developmental Engineering, School of Agriculture, Meiji University, 1-1-1 Higashimita, Tama, Kawasaki, Japan. [2]Meiji University International Institute for Bio-Resource Research (MUIIBR), 1-1-1 Higashimita, Tama, Kawasaki, Japan. [3]Department of Orthopaedic Surgery, Surgical Science, Tokai University School of Medicine, 143 Shimokasuya, Isehara, Kanagawa, Japan. [4]Laboratory of Microbial Genetics, School of Agriculture, Meiji University, 1-1-1 Higashimita, Tama, Kawasaki, Japan. [5]School of Materials Science, Japan Advanced Institute of Science and Technology, 1-1 Asahidai, Nomi, Ishikawa, Japan. [6]Center for Fiber and Textile Science, Kyoto Institute of Technology, Creation Core Kyoto Mikuruma 213, Kamigyo, Kyoto, Japan.

Received: 17 April 2013 Accepted: 22 July 2013
Published: 25 July 2013

References

1. Yamato M, Okano T: **Cell sheet engineering.** *Mater Today* 2004, **7**(5):42–47.
2. Elloumi-Hannachi I, Yamato M, Okano T: **Cell sheet engineering: a unique nanotechnology for scaffold-free tissue reconstruction with clinical applications in regenerative medicine.** *J Intern Med* 2010, **267**(1):54–70.
3. Yamada N, Okano T, Sakai H, Karikusa F, Sawasaki Y, Sakurai Y: **Thermo-responsive polymeric surfaces; control of attachment and detachment of cultured cells.** *Macromol Rapid Commun* 1990, **11**:571–576.
4. Nishida K: **Tissue engineering of the cornea.** *Cornea* 2003, **22**(Suppl 7):28–34.
5. Yamato M, Utsumi M, Kushida A, Konno C, Kikuchi A, Okano T: **Thermo-responsive culture dishes allow the intact harvest of multilayered keratinocyte sheets without dispase by reducing temperature.** *Tissue Eng* 2001, **7**(4):473–480.
6. Ohki T, Yamato M, Murakami D, Takagi R, Yang J, Namiki H, Okano T, Takasaki K: **Treatment of oesophageal ulcerations using endoscopic transplantation of tissue-engineered autologous oral mucosal epithelial cell sheets in a canine model.** *Gut* 2006, **55**(12):1704–1710.
7. Shiroyanagi Y, Yamato M, Yamazaki Y, Toma H, Okano T: **Urothelium regeneration using viable cultured urothelial cell sheets grafted on demucosalized gastric flaps.** *BJU Int* 2004, **93**(7):1069–1075.
8. Shimizu T, Yamato M, Kikuchi A, Okano T: **Two-dimensional manipulation of cardiac myocyte sheets utilizing temperature-responsive culture dishes augments the pulsatile amplitude.** *Tissue Eng* 2001, **7**(2):141–151.
9. Shimizu T, Sekine H, Isoi Y, Yamato M, Kikuchi A, Okano T: **Long-term survival and growth of pulsatile myocardial tissue grafts engineered by the layering of cardiomyocyte sheets.** *Tissue Eng* 2006, **12**(3):499–507.
10. Akizuki T, Oda S, Komaki M, Tsuchioka H, Kawakatsu N, Kikuchi A, Yamato M, Okano T, Ishikawa I: **Application of periodontal ligament cell sheet for periodontal regeneration: a pilot study in beagle dogs.** *J Periodontal Res* 2005, **40**(3):245–251.
11. Kaneshiro N, Sato M, Ishihara M, Mitani G, Sakai H, Mochida J: **Bioengineered chondrocyte sheets may be potentially useful for the treatment of partial thickness defects of articular cartilage.** *Biochem Biophys Res Commun* 2006, **349**(2):723–731.
12. Ito S, Sato M, Yamato M, Mitani G, Kutsuna T, Nagai T, Ukai T, Kobayashi M, Kokubo M, Okano T, *et al*: **Repair of articular cartilage defect with layered chondrocyte sheets and cultured.** *Biomaterials* 2012, **33**(21):5278–5286.
13. Nishida K, Yamato M, Hayashida Y, Watanabe K, Yamamoto K, Adachi E, Nagai S, Kikuchi A, Maeda N, Watanabe H, *et al*: **Corneal reconstruction with tissue-engineered cell sheets composed of autologous oral mucosal epithelium.** *N Engl J Med* 2004, **351**(12):1187–1196.